

# Electrocatalytic Reduction of Oxygen at Binderless Carbon-Pt Nanostructured Electrodes: Effects of the Nature of the Carbon Support and the Pt Morphology

Zéhira Hamoudi, Brahim Aïssa, My Ali El Khakani and Mohamed Mohamedi\*

Institut National de la Recherche Scientifique (INRS)-Énergie, Matériaux et Télécommunications (EMT), 1650 Boulevard Lionel Boulet, Varennes, Québec, J3X 1S2, Canada.

\*E-mail: [mohamedi@emt.inrs.ca](mailto:mohamedi@emt.inrs.ca)

Received: 4 October 2012 / Accepted: 22 October 2012 / Published: 1 December 2012

---

This work discusses the effect of the carbon morphology in binderless nanostructured Pt catalyst on the oxygen reduction reaction (ORR). In summary, we have examined five type of carbon, the carbon paper (CP), carbon sphere chains (CSC), carbon nanofibers (CNF), carbon nanotubes (CNT) and carbon nanohorns (CNH). On the surface of each carbon, Pt was deposited by considering three morphologies, well-spread nanoparticles, smooth film and porous film. In a deaerated H<sub>2</sub>SO<sub>4</sub> solution, highly interconnected Pt NPs (smooth film and columnar-like arranged NPs) displayed weakened oxophilicity as compared with spread Pt NPs. In O<sub>2</sub>-saturated 0.5 M H<sub>2</sub>SO<sub>4</sub> solutions, the onset potential and half-wave potential for the ORR imply that Pt supported by carbons of tubular form such as the CNF, CNT or CNH are superior catalyst supports. More markedly, it seems that the dimensions (diameter and length) is irrelevant since the three carbons (CNF, CNT, CNH) displayed similar supporting properties regarding either the onset potential or the half-wave potential of ORR.

---

**Keywords:** Platinum; carbon nanostructures; morphology effect; oxygen electroreduction

## 1. INTRODUCTION

The oxygen reduction reaction ORR is among the most widely investigated electrochemical reaction, as it is of great importance to many electrochemical practical applications including fuel cells [1-3]. Until today, Pt is known as the most active catalyst towards the ORR. However, the high overpotential of the ORR and the high cost of Pt restrict its commercial use as a catalyst. Less expensive catalysts with performance similar or higher than Pt have not emerged yet despite intense research efforts conducted throughout the world [4].

It is expected that nanostructuring the catalyst will lead to better utilization of noble metal and hence low electrode costs. Nevertheless, even as nanometric form, the activity of electrode catalysts in fuel cell applications will depend strongly on the nature of the catalyst support, its electrical conductivity, ability to provide high dispersion for the catalyst nanoparticles, and its durability [5-6].

In most fuel cell electrode configurations, carbon black (CB) in powder form mixed with a binder is used as the catalyst support. However, it has been demonstrated that CB could be corroded (or oxidized) under the severe system-imposed operating conditions [7-8]. The attention has then been focused on carbon nanostructures (CNS) forms such as carbon nanofibers (CNF) and carbon nanotubes (CNT) owing to their resistance to oxidation and high electronic conductivity, which makes them superior supports to the traditional CB [5,9].

In recent years, we have been developing free-standing (binderless) nanostructured catalyst layers as anodes for the electrooxidation of alcohols such as methanol and ethanol for direct alcohol fuel cells. In such structures, in addition to the catalyst we also investigated carbon supports of different geometries such as CNF [10], carbon sphere chains (CSC) [11-12], CNT [13-14], carbon nanohorns (CNH) [15] and carbon paper (CP) [16] on the performance of the anode. Of these studies, we have shown that the morphology of the carbon plays a non-trivial role on the electroactivity of the anode, i.e., the CNH and CNT displayed the highest electrocatalyst supporting properties towards methanol and ethanol electrooxidation, respectively.

Similarly for ORR, it can be expected that geometrical structure of the carbon support will play an important role on the performance of the cathode. This work represents the first comparative assessment on the effect of the carbon structure support in the binderless Pt electrode on the potential of ORR. Binderless electrodes permit to evaluate the role of the nature of the carbon support in neat form without the interference of binders or any other additives found in conventional electrodes.

The main focus in this work was to assess the onset potential and the half-wave potential of ORR at five carbon electrocatalyst supports, namely, CP, CSC, CNF, CNT and CNH. Onto each carbon structure, Pt catalyst was deposited in three morphologies that are spread nanoparticles NPs, smooth thin film (closed structure) and columnar-organized NPs (porous structure).

## **2. EXPERIMENTAL**

### *2.1. Materials synthesis*

The synthesis and full physical-chemical characterizations of the carbon structures used here are reported elsewhere, CNF [10], CNT [13-14], CNH [15] and CSC [12]. All the carbon structures were grown onto an electrically conductive carbon microfibers substrate (current collector).

Pt in various morphology was deposited by pulsed laser deposition (PLD) and full details and characterization are reported [13, 16].

### *2.2. Electrochemical studies*

Electron transfer properties of the carbon structures as-well as their Pt decorated counterparts were assessed by cyclic voltammetry (CV) in 0.5 M H<sub>2</sub>SO<sub>4</sub> and O<sub>2</sub>-saturated 0.5 M

H<sub>2</sub>SO<sub>4</sub> solutions. All measurements were conducted at room temperature using a three-electrode cell with the reference electrode and counter electrode being an Ag/AgCl, 3 M NaCl and a platinum coil, respectively. The reference electrode was separated from the analyte solution by a Luggin capillary that is very close to the working electrode to minimize the *IR* drop. Measurements and data acquisition were conducted with a potentiostat/galvanostat Autolab from EcoChemie.

### 3. RESULTS AND DISCUSSIONS

#### 3.1. Electrode structures

The binderless CNS/Pt electrode structures studied in this work are shown in Fig. 1. The five different carbons morphologies were:

(i) Commercial Carbon paper (CP, Toray) made of 3D network of carbon fibers with an average diameter of 8  $\mu$ m. This type of CP has a considerable open space (porosity) and is most used as the substrate onto which the catalyst layer is deposited in the area of fuel cells.

(ii) Solid carbon spheres chains with spheres having a diameter varying between 200 and 1000 nm (average of  $680 \pm 60$  nm). All the carbon spheres are intimately connected to each other forming chain-like compounds in several microns in length [12].

(iii) Carbon nanofibers having an average length higher than 20  $\mu$ m and average outer diameter of 250 nm. The inner structure of these CNFs is hollow of the herringbone type [10].

(iv) Carbon nanotubes with lengths exceeding tens of micrometers and outer diameter varying between 7 and 18 nm with a maximum at around 12.5 nm [13,18].

(v) Carbon nanohorns that resembles to carbon nanofilaments ( $\sim 10$  nm-diam. and with lengths above 0.5  $\mu$ m). TEM analysis revealed that CNHs are characterized by a tubular diameter in the 2-4 nm range, a length in the 10-30 nm range and cone angles in the 20-30° range [15].

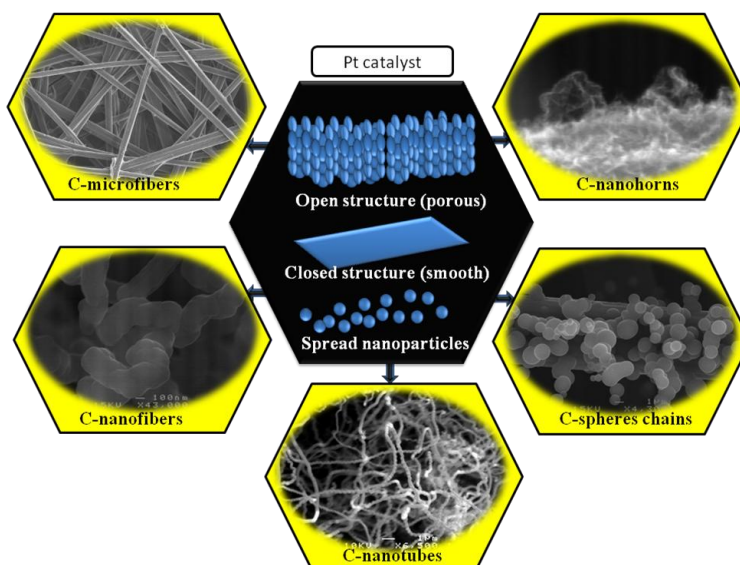


**Figure 1.** SEM images of the five morphologies of carbon studied in this work. Centre is a rough representation of the different morphologies of Pt catalysts deposited onto each carbon.

Figure 1 (centre part) shows a rough representation of the various morphologies of the Pt catalyst deposited onto the five types of carbon. Namely, Pt catalyst was deposited in three morphologies: (i) well spread nanoparticles NPs (with no agglomeration and generally isolated with little interconnection), (ii) dense and smooth thin film (closed structure) and (iii) porous thin film (columnar arrangement of the NPs). The Pt smooth film and Pt porous film had a thickness around 50 nm and are denoted here Pt50 and Pt50p (p stands for porous), respectively. The average particle diameter was estimated to be 1.6 for Pt NPs and roughly 3 nm for both Pt50 and Pt50p. Details regarding the physico-chemical characterization of the three Pt morphologies are reported elsewhere [13,16].

### 3.2. Electrochemical behaviour in acidic solution

Figure 2a, shows representative CV run at CNT/Pt50p electrode in 0.5 M H<sub>2</sub>SO<sub>4</sub> deaerated solution at a potential scan rate of 50 mV/s. First, it can be seen that the electrode exhibited the very well-known hydrogen adsorption (H<sub>ads</sub>) and desorption (H<sub>des</sub>) regions in the potential region of ca. -0.2 to 0 V vs. Ag/AgCl and Pt oxide formation and reduction within ca. 1.1 to 0.4 V vs. Ag/AgCl [19-20].

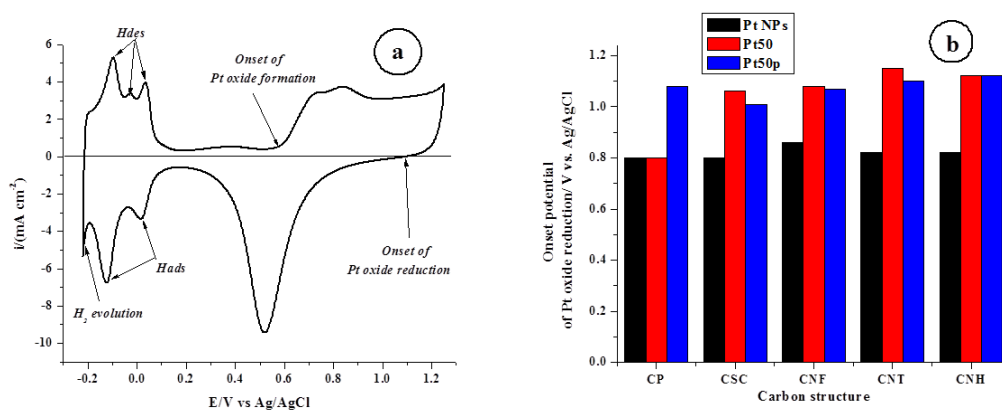


**Figure 2.** (a) Typical cyclic voltammetry in 0.5 M H<sub>2</sub>SO<sub>4</sub> solution with the scan rate of 50 mV/s recorded at CNT/Pt50p electrodes. (b) Summary of the onset potential of Pt oxide reduction at the different CNS/Pt electrodes.

The onset potential of reduction of Pt oxide is a parameter of particular interest to study the ORR because it provides information regarding the interaction of the catalyst with oxygen-containing species. Fig. 2b summarizes the onset potential of reduction of Pt oxide at the various CNS/Pt electrodes in a deaerated solution of H<sub>2</sub>SO<sub>4</sub> similar to conditions reported in Fig. 2a. At the Pt NPs supported electrodes, the onset potential of reduction of Pt oxide is around 0.8 V irrespective of the nature of the carbon support. On the other hand, at thicker Pt layer (Pt50 and Pt50p) it is more positive and slightly oscillate between 1.0 and 1.1 V independently of the nature of the carbon support. So, it looks that the Pt morphology (smooth vs porous) has no effect on the onset potential of Pt oxide reduction. Still, compared to CNS/Pt NPs, the more positive onset potential of reduction of Pt oxide

exhibited by CNS/Pt50 and CNS/Pt50p indicates reduced oxophilicity, meaning a weakened chemical adsorption energy with oxygen-containing species. We ascribe this behaviour to the effect of the Pt loading  $0.69 \text{ mg/cm}^2$  (Pt50 and Pt50p) vs  $0.18 \text{ mg/cm}^2$  (Pt NPs). Higher Pt loading induce higher interconnectivity of Pt NPs which is the case here with Pt50 and Pt50p. This is in line with the observations of Wang et al. who also proposed that interconnected Pt NPs would significantly weaken their chemical adsorption with oxygen-containing species [21].

### 3.3. Oxygen reduction reaction

Typical representative CVs recorded at CNF/Pt NPs electrode in  $0.5 \text{ M H}_2\text{SO}_4$  solution with and without  $\text{O}_2$  are shown in Fig. 3. In the absence of  $\text{O}_2$ , only a small current background can be observed. In the presence of  $\text{O}_2$  a very large reduction wave starting at ca.  $0.65 \text{ V}$  (the onset potential) followed by a cathodic limiting current within  $0.3 \text{ V}$  and  $0 \text{ V}$  vs Ag/AgCl. The cathodic current flowing during the reduction of oxygen should also comprise the current of the reduction of platinum oxide. It is not possible to distinguish these two contributions precisely. Nevertheless, the cathodic currents of  $\text{O}_2$  reduction under present conditions were much larger than the current of platinum oxide reduction, which is confirmed from the cathodic current in argon-saturated solution (Fig. 3, black curve). Therefore, it is safe to assert that the major contribution of the cathodic current in  $\text{O}_2$ -saturated solution resulted from  $\text{O}_2$  reduction.

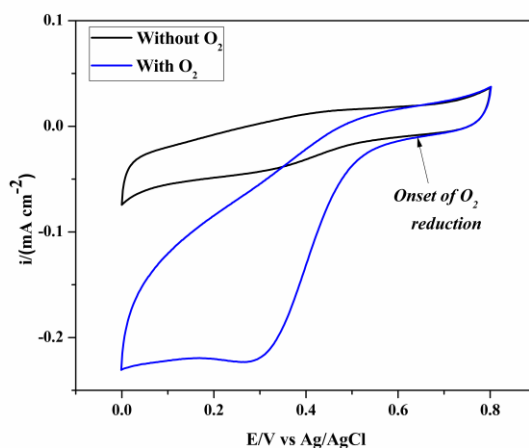


**Figure 3.** (a) Typical cyclic voltammetry at CNF/Pt NPs electrode in a deaerated  $0.5 \text{ M H}_2\text{SO}_4$  solution (black curve) and  $0.5 \text{ M H}_2\text{SO}_4$ -oxygen saturated solution (blue line) with the scan rate of  $50 \text{ mV/s}$ .

Figure 4 reports the linear scan voltammetric (LSVs) curves for the ORR measured in  $\text{O}_2$ -saturated  $0.5 \text{ M H}_2\text{SO}_4$  at (a) CP/Pt, (b) CSC/Pt, (c) CNF/Pt, (d) CNT/Pt and (e) CNH/Pt electrodes. It is obvious that each electrode system catalyses the reduction of oxygen to a different extent. It is interesting to first note that for a given carbon structure, the catalytic activity towards the ORR follows

Pt50p>Pt50>Pt NPs. We have observed similar trend regarding methanol electrooxidation [11, 13] which was explained by the fact that Pt NPs exist as isolated particles and the distance between the particles is likely to induce a high impedance for charge transfer from particle to particle. Then, the increase of interconnectivity of Pt nanoparticles (Pt50 and Pt50p) reduces the interface resistance among particles for electron charge transfer. Finally, the high electrocatalytic activity of Pt50p is believed to be linked to the increased porosity (high surface area) and to the columnar arrangement of the NPs, which provide better accessibility to the electrolyte and by that better utilization of the Pt catalyst.

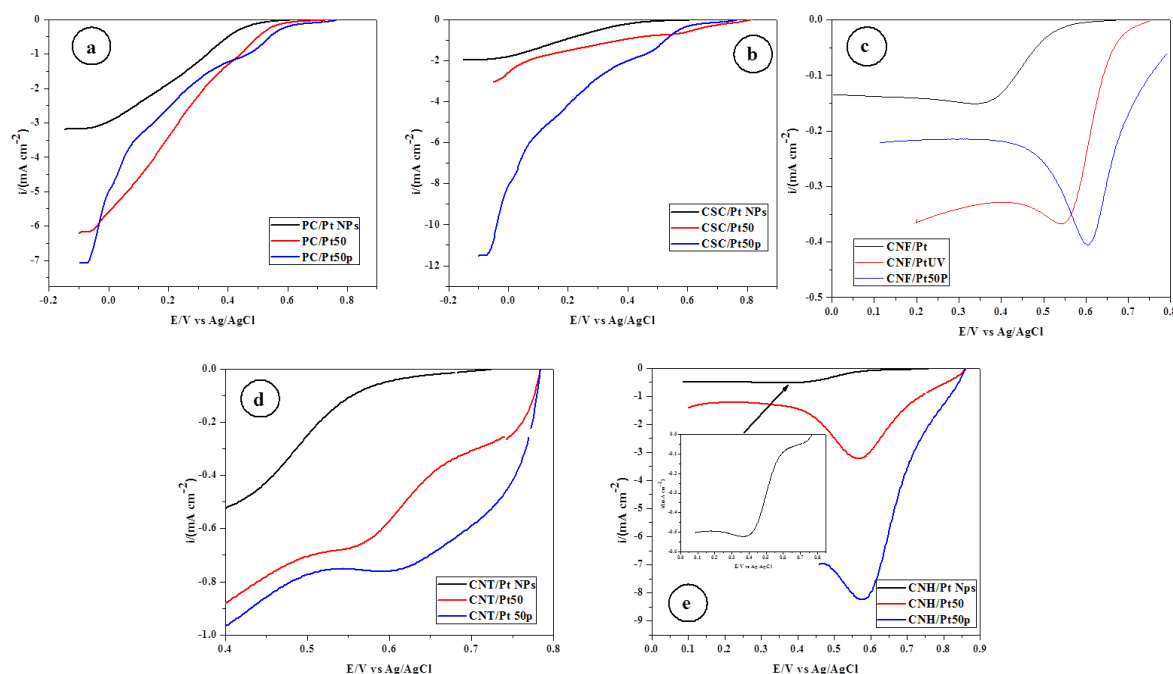


**Figure 4.** (a) Typical LSVs at CNS/Pt electrodes in an 0.5 M H<sub>2</sub>SO<sub>4</sub>-oxygen saturated solution with the scan rate of 50 mV/s. (a) CP/Pt, (b) CSC/Pt, (c) CNF/Pt, (d) CNT/Pt and (e) CNH/Pt.

Now is there an effect of the carbon morphology support on the electroactivity towards ORR for a given Pt morphology? Figure 4 shows that this is the case. Indeed, the LSVs at CP/Pt CSC/Pt electrodes exhibited control regions of kinetic, mixed and diffusion limited (Fig. 4a-b). The reduction current gradually increased and reached a plateau at potentials within -0.1 and -0.15 V close to H<sub>2</sub> evolution. On the other hand for the carbon of tubular form CNF/Pt NPs (Fig. 5c), CNT/Pt NPs (Fig. 5d) and CNH/Pt NPs (Fig. 5e) displayed clear S-shaped curves with a reduction plateau at more positive potentials (within 0.5 and 0.3 V range). For higher Pt loading (Pt50 and Pt50p) the LSVs are shifted to more positive potentials and the S-shape of the LSV transforms into a more or less peak-shaped one (Fig. 5c-e) indicating diffusion control at positive potentials.

The onset potential of ORR provides indication on the electroactivity [22]. In order to compare the ORR activities of the CNS/Pt electrodes, the onset potentials for the ORR extracted from Fig. 4 are summarized in Fig. 5 for each Pt morphology as function of the carbon support. For higher Pt loadings

(Pt50 and Pt50p) (Fig. 5b and 5c), the results show that irrespective of the nature of the carbon support, there is no significant difference in the onset potential of ORR which situates between 0.72 V and 0.79 V. On the other hand, there is a clear effect of the carbon support on Pt NPs catalyst (Fig. 5a). The tubular carbons (CNF, CNT, and CNH)/Pt NPs showed an onset potential more positive (between 0.67 and 0.71 V) than the CP/Pt NPs (0.54 V) or CSC/Pt NPs (0.62 V). These first observations suggest that ORR is more active at Pt supported by tubular carbon structure whatever the Pt morphology.

The half-wave potential,  $E_{1/2}$  is another parameter that permits to assess further the electroactivity towards the ORR [23]. Figure 5d resumes the  $E_{1/2}$  also extracted from Fig. 4. It can be seen that Pt NPs catalyst showed the most negative  $E_{1/2}$  regardless of the carbon structure. As the Pt loading increased,  $E_{1/2}$  became more positive. As explained before with the results obtained in a deaerated 0.5 M  $H_2SO_4$  solution (section 3.2.), the shift in  $E_{1/2}$  for ORR to higher positive potentials is due to the lessened coverage of oxide/hydroxide on the Pt surface at high potentials, providing a larger number of reaction sites as observed in sulfuric acid solution. The most positive  $E_{1/2}$  is obtained with Pt50p supported on carbon of nanotubular forms (CNF, CNT, and CNH). The  $E_{1/2}$  recorded at these three electrode structure is almost similar (1 mV of difference at the most) and is around 0.69 V vs. Ag/AgCl.

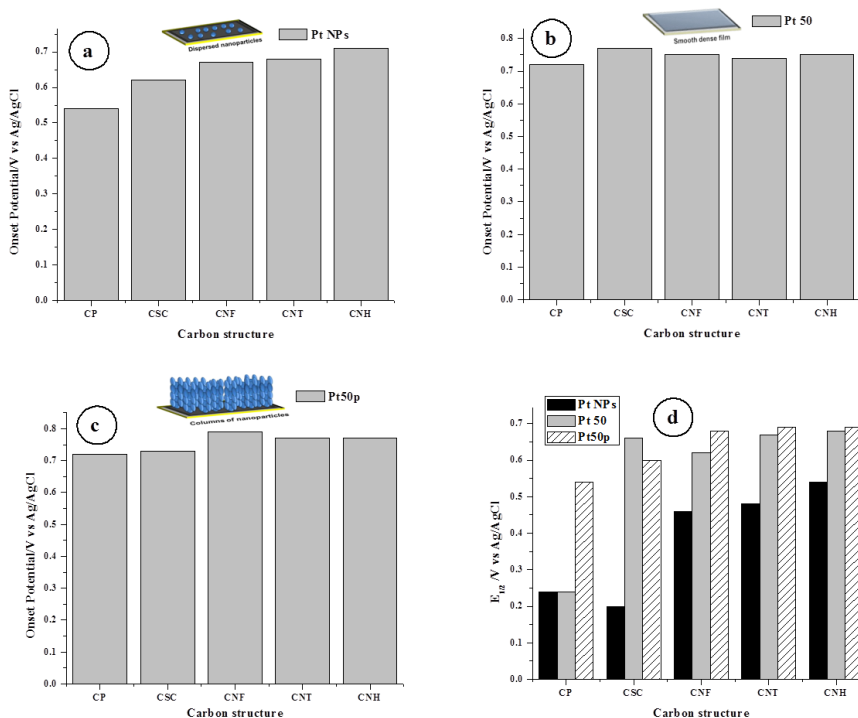


**Figure 5.** Onset potential for ORR at CNS/Pt electrodes: (a) CNS/Pt NPs, (b) CNS/Pt50, (c) CNS/Pt50p, and (d) Summary of the half-wave potential for ORR at the different CNS/Pt electrodes.

The analysis of the onset potential and  $E_{1/2}$  suggests that high electroactivity towards ORR is obtained with Pt50p which is due to the porous nature of the Pt film. Interestingly, this high electroactivity was similar with three carbon structure that are the CNF, CNT and CNH.

From an economical point of view, CNF and CNT are cheaper to fabricate since it necessitate the use of the chemical vapor deposition technique, which is a cost-effective method. On the contrary, CNH are synthesized using laser ablation techniques that still very expensive.

#### 4. CONCLUSIONS

The prime objective of this paper is to investigate the effect of the nature of the carbon support on the potential of oxygen reduction reaction. Towards that aim five carbon morphologies that are CP, CSC, CNF, CNT and CNH were studied. Each of the carbon was decorated with Pt catalyst in a binderless electrode construction in order to assess the effect of the carbon support in neat form. Pt catalyst was deposited in three different morphologies, i.e., well-dispersed NPs, smooth film and porous film. Some important observations could be drawn from this first part of study:

In  $\text{H}_2\text{SO}_4$  solution, highly interconnected Pt NPs (smooth film and columnar-like arranged NPs) displayed reduced oxophilicity as compared with spread Pt NPs.

Comparison of the response seen for the oxygen reduction reaction suggests that Pt supported by carbons of tubular form such as the carbon nanofibers, carbon nanotubes or carbon nanohorns are better catalyst supports compared to microfibrinous carbon paper or the carbon sphere chains. More importantly, within the different tubular forms of carbon, it seems that the dimensions (diameter and length) are irrelevant since the three carbons (CNF, CNT, CNH) displayed similar supporting properties regarding either the onset potential or the half-wave potential of ORR. These behaviours are not understood from the theoretical point of view and further work is needed by means of theoretical modelling considering the morphology of the carbon altogether with the ORR.

Now, are the dimensions of the tubular carbon also unimportant on the current mass activity? This question needs to be answered by performing cyclic voltammetry under steady-state conditions particularly near the half-wave potential. Work is underway to construct and adapt our samples for rotating-disk electrode system and results will be reported in due course.

#### ACKNOWLEDGEMENT

This work was supported by the Natural Sciences Engineering Research Council of Canada (NSERC), the Centre Québécois sur les Matériaux Fonctionnels (CQMF), the FQRNT and the MDEIE.

#### References

1. A. Nozad Golikand and L. Irannejad, *Electroanalysis* 20, (2008) 1121.
2. Drew C. Higgins, D. Meza, and Z. Chen, *J. Phys. Chem. C* 114 (2010) 21982.
3. Y. Bing, H. Liu, L. Zhang, D. Ghosh and J. Zhang, *Chem. Soc. Rev.* 39 (2010) 2184.
4. A. Morozan, B. Joussetme and S. Palacin, *Energy Environ. Sci.* 4 (2011) 1238.
5. C. Wang, M. Waje, X. Wang, J. M. Tang, R. C. Haddon, Y. S. Yan, *Nano Lett.* 4 (2004) 345.
6. R. Giorgi, L. Giorgi, S. Gagliardi, E. Salernitano, M. Alvisi, Th. Dikonimos, N. Lisi, D. Valerini, M. F. De Riccardis, E. Serra, *J. Fuel Cell Sci. Technol.* 8 (2011) 041004.

7. Y. Shao, J. Wang, R. Kou, M. Engelhard, J. Liu, Y. Wang, Y. Lin, *Electrochim. Acta* 54 (2009) 3109.
8. P. J. Ferreira, G. J. la O', Y. Shao-Horn, D. Morgan, R. Makharia, S. Kocha, and H. A. Gasteiger, *J. Electrochem. Soc.* 152 (2005) A2256.
9. T. Matsumoto, T. Komatsu, K. Arai, T. Yamazaki, M. Kijima, H. Shimizu, Y. Takasawa and J. Nakamura, *Chem. Commun.* 840 (2004).
10. Z. Hamoudi, M. A El Khakani, M. Mohamedi, *Int. J. Hydrogen Energy* 36 (2011) 4682.
11. Z. Hamoudi, M. A. El Khakani, and M. Mohamedi, *Electroanalysis* 23 (2011) 1205.
12. Z. Hamoudi, B. Aissa, M. A. El Khakani, M. Mohamedi, *J. Phys. Chem. C*, 114 (2010) 1885.
13. Z. Hamoudi, M. A. El Khakani and M. Mohamedi, *J. Electrochem. Soc.* 159 (2012) B331.
14. Amel Tabet-Aoul and M. Mohamedi, *J. Mater. Chem.* 22 (2012) 2491.
15. B. Aissa, Z. Hamoudi, T. Hiro, K. Tohji, M. Mohamedi, M. A. El Khakani, *Electrochem. Comm.* 11 (2009) 862.
16. Z. Hamoudi, M A. El Khakani, and M. Mohamedi *Int. J. Electrochem. Sci.* 7 (2012) 1666.
17. W. Xu, X. Zhou, C. Liu, W. Xing, Ti. Lu, *Electrochem. Comm.* 9 (2007) 1002.
18. A. Tabet-Aoul, F. Saidani, D. Rochefort and M. Mohamedi, *Int. J. Electrochem. Sci.* 6 (2011) 6385.
19. K. Kinoshita, D. R. Ferrier, and P. Stonehart, *Electrochim. Acta* 23 (1978) 45.
20. T. J. Schmidt, H. A. Gasteiger, G. D. Stab, P. M. Urban, D. M. Kolb, and R. J. Behm, *J. Electrochem. Soc.* 145 (1998) 2354.
21. S. Wang, S. P. Jiang, T. J. White, J. Guo, and X. Wang, *J. Phys. Chem. C* 113 (2009) 18935.
22. A. Sarapuu, M. Nurmik, H. Mändar, A. Rosental, T. Laaksonen, K. Kontturi, D. J. Schiffrin, K. Tammeveski, *J. Electroanal. Chem.* 612 (2008) 78.
23. R. R. Adzic, J. Zhang, K. Sasaki, M. B. Vukmirovic, M. Shao, J. X. Wang, A. U. Nilekar, M. Mavrikakis, J. A. Valerio, F. Uribe, *Top Catal* 46 (2007) 249.